Rare Metal Materials and Engineering
Volume 45, Issue 6, June 2016
Online English edition of the Chinese language journal

Available online at www.sciencedirect.com
ScienceDirect

Cite this article as: Rare Metal Materials and Engineering, 2016, 45(6): 1413-1418.

ARTICLE

Effect of Rare Earth Element Yttrium on the Isothermal Oxidation Behavior of Aluminide Coatings on Ti-Ni Shape Memory Alloys

Xu Jiawen, Liu Ailian, Wang Yongdong, Zhou Yuebo

Heilongjiang University of Science and Technology, Harbin 150022, China

Abstract: Ti-Ni shape memory alloys with and without Y addition were aluminized at 650 ℃ using a pack-cementation method. The influences of various amounts of Y additions on the microstructure and the isothermal oxidation behaviors of aluminide coatings in air at 700 ℃ were investigated. The results show that aluminide coatings exhibit double layer structure, and the aluminization process is mainly controlled by the inner diffusion of Al. The Y addition promotes the growth of outer $TiAl_3$ layer, but it retards the growth of inner $NiAl_3$ layer when Y content is lower than 1at%. Isothermal oxidation results indicate that the scale growth rate is significantly reduced when the Y addition is 0.5at%. In contrast, the oxidation rate of Ti-Ni alloy is increased when 1at% Y and 5at% Y are added, especially 5at% Y addition. The effect of Y element on the coating formation and the coating oxidation behavior was discussed.

Key words: shape memory alloy; aluminide; isothermal oxidation; active element effect; rare earth Y

Near equal-atomic Ti-Ni (Ni-45wt%Ti) shape memory alloys (SMAs) are technologically important materials because of their outstanding shape memory effect (SME) and superelasticity[1]. Up to now the application of Ti-Ni SMAs has been spread to aerospace, aviation and other fields involving the exposure to high temperatures. Thus, oxidation is an unavoidable problem when Ti-Ni SMAs are exposed to air for a long period. The oxidation causes significant changes in the microstructure of the shape memory alloy, e.g., destabilization of martensite phase, and as a result, the shape memory effect of the alloy diminishes[2]. At the same time, shape memory alloys need to be heat-treated for rearrangement of the crystal structure, and the process of the heat treatment will also cause oxidation[2-6]. In previous works, the authors[7] found that the addition of Y not only enhanced the martensitic transformation temperature of Ti-Ni alloys, but also improved their oxidation resistance, which was referred to as "reactive element effect" (REE)[8]. Various theories have been put forward to elucidate the REE but still are in dispute[9]. In order to improve the oxidation resistance of Ti-Ni alloy, different surface treatments were proposed. Aluminization at low temperature by pack cementation can increase the high temperature oxidation resistance[10-13]. However, there is no report about the oxidation of low temperature aluminide coatings on Ti-Ni alloys with or without Y addition. The aim of this research is to study the effect of Y addition on the isothermal oxidation behavior of low temperature aluminide coatings formed on Ti-Ni alloys, which will be of benefit to their application.

1 Experiment

Samples with dimension of 15 mm×10 mm×2 mm were cut from $Ti_{50}Ni_{50}$, $Ti_{49.75}Ni_{49.75}Y_{0.5}$, $Ti4_{9.5}Ni_{49.5}Y_1$, and $Ti_{47.5}Ni_{47.5}Y_5$ alloys ingots, which were prepared by a

Received date: June 03, 2015
Foundation item: National Natural Science Foundation of China (51201062, 51371078)
Corresponding author: Liu Ailian, Ph. D., Associate Professor, College of Materials Science and Engineering, Heilongjiang University of Science and Technology, Harbin 150022, P. R. China, Tel: 0086-451-88036159, E-mail: liuailian@yeah.net

non-consumable arc-melting furnace under an argon atmosphere using a water-cooled copper crucible. The details of alloy production process were reported elsewhere[7]. The samples were ground to a final 800# SiC paper. After ultrasonically cleaning in acetone, they were aluminized using a conventional pack cementation in a homogeneous mixture of 75wt%Al+20wt% Al_2O_3+5wt% NH_4Cl in a pure Ar atmosphere at 650 ℃ for 6 h. Afterwards, the samples were brushed, cleaned in bubbling distilled water for 30 min and then ultrasonically cleaned in acetone to remove loosely embedded pack particles. For the convenience of narration, the aluminide coatings formed on $Ti_{50}Ni_{50}$, $Ti_{49.75}Ni_{49.75}Y_{0.5}$, $Ti_{49.5}Ni_{49.5}Y_1$, and $Ti_{47.5}Ni_{47.5}Y_5$ (at%) were denoted as Y0, Y0.5, Y1 and Y5, respectively.

The oxidation experiments were carried out in air at 700 ℃ for up to 50 h and the mass measurements were conducted after fixed time intervals using a balance with 0.01 mg sensitivity. The compositions and phases of the various aluminide coatings before and after oxidation were investigated using Camscan MX2600FE type scanning electron microscopy (SEM) with an energy dispersive spectroscope (EDS) and D/Max-2500 pc type X-ray diffraction (XRD). Electroless Ni-plating was coated on the surface of the oxidized specimens to prevent the spallation of the scales during the process of specimen preparing for observing the morphologies of the cross-sections.

2 Results and Discussion

2.1 Microstructure

Previous results[7] indicated that the addition of Y refined the grains of the Ti-Ni alloy. This is because of the formed Y-enriched NiY particles, which not only promoted the nucleation of new crystals during casting, but also suppressed the growth of Ti-Ni grains during heat-treatment. Moreover, the fraction of NiY particles increases with the increase of Y content.

The aluminide coatings were prepared by pack cementation at 650 ℃ for 6 h. The average concentration of Al element in the surface zone (<4 μm: the profile depth of electron beam) is close to 61.2wt% for three aluminide coatings on a basis of EDS area analysis. Fig.1 shows the XRD patterns of Ti-Ni-Y alloys. It can be seen from Fig.1 that all aluminide coatings only contain two intermetallic phases: $TiAl_3$ and $NiAl_3$ phase. According to Ti-Ni binary phase diagram[14], the solubility of Ti in Ni is 21.4wt%, but the solubility of Ni in Ti is 38wt%. Thus, both $TiAl_3$ and $NiAl_3$ phases in the present paper should be Ti(Ni)Al_3 and Ni(Ti)Al_3 solid solutions, respectively.

Fig.2 shows the corresponding cross-sectional morphologies and elemental profiles of various aluminide coatings developed on Ti-Ni alloys with and without Y addition. Clearly, a double layer (termed as "Ⅰ" and "Ⅱ") with different thicknesses is formed on all aluminide

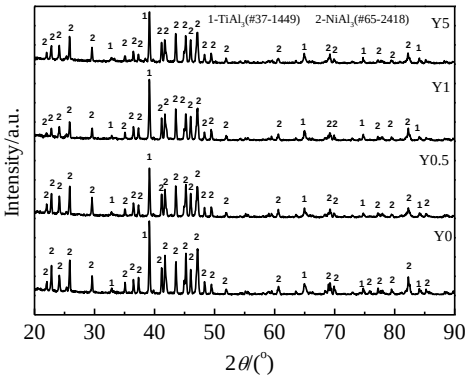

Fig.1 XRD patterns of Ti-Ni-Y alloys after aluminized

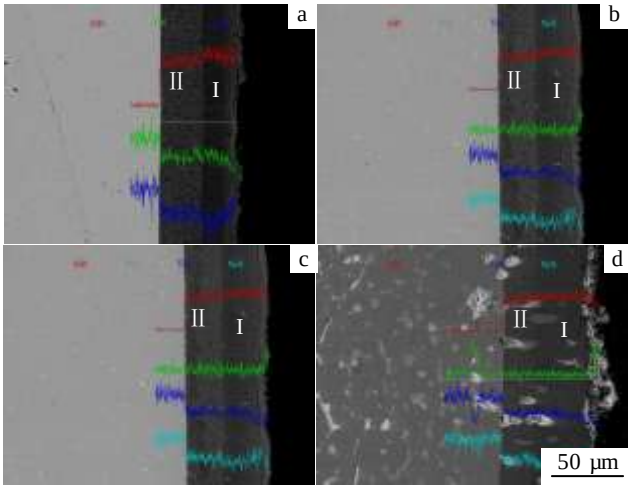

Fig.2 Cross-sectional images and elemental depth profiles of various samples: (a) Y0, (b) Y0.5, (c) Y1, and (d) Y5

coatings, as shown in Fig.2 and listed in Table 1. Element profiles results indicate that the outer layer has higher Al content than the inner layer. Based on the results of XRD patterns and Fig.2, it can be concluded that the phase in region "Ⅰ" is mainly $TiAl_3$ phase while that in region "Ⅱ" is mainly $NiAl_3$ phase. It is noteworthy that the bright phase in the aluminide coatings is composed of the dispersed Y-richen particles, which are from the original Y-richen NiY particles in Ti-Ni alloy[7]. In Table 1, it is clearly shown that the thickness of outer $TiAl_3$ layer increases with the increscent of Y content, but the thickness of inner $NiAl_3$ layer decreases with the increscent of Y content when Y content is below 1at%. In other words, the highest thickness ratio of outer $TiAl_3$ layer to inner $NiAl_3$ layer occurs on sample Y1.

Fig.2 shows that the aluminide coatings have double-layered microstructure: the outer $TiAl_3$ layer and the inner $NiAl_3$ layers. The distribution of Y-rich NiY particles,

Table 1 Thickness of aluminide coating, interdiffusion zone and outdiffusion zone after oxidation

Sample		Y0	Y0.5	Y1	Y5
Aluminide coating	Ⅰ	28 μm	39 μm	53.3 μm	45.6 μm
	Ⅱ	37 μm	30.5 μm	24.7 μm	26 μm
	Ⅰ + Ⅱ	65 μm	69.5 μm	78 μm	71.6 μm
	Ⅰ / Ⅱ	0.76	1.28	2.16	1.75
Interdiffusion zone	Ⅴ (Ti rich)	2 μm	1.5 μm	1.5 μm	
	Ⅳ (Al rich)	6.5 μm	4.5 μm	4.5 μm	
Ⅵ (outer diffusion zone)		18 μm	12 μm	22 μm	

which can be regarded as inert marks, further indicates that the aluminization progress is mainly controlled by inward diffusion of Al. The aluminization progress can be addressed as below. At high temperature, the inner diffusion of Al causes the formation of the surface $TiAl_3$ phase within Ni solution. Due to the lower solubility of Ni in $TiAl_3$ phase than that in origin Ti-Ni alloy, Ni in surface $TiAl_3$ layer will diffuse inwardly to form a Ni-rich layer. When Al diffuses into the Ni-rich layer, $NiAl_3$ inner layer with Ti solution is formed. With the increase of reaction time, the thicknesses of both layers increase. However, from Table 1, it is clear that the addition of Y accelerates the growth of outer $TiAl_3$ layer, but retards the growth of inner $NiAl_3$ layer when the content of Y is below 1at%. The higher amount of Y-rich particles close to Ti-Ni base/$NiAl_3$ interface than that in other places suggests that Y-rich particles also move inward. In longer time, a Y-rich layer diffusion barrier will be formed. Zhou et al[12] and Tan et al[15] observed the same phenomenon during the aluminization of Ni-CeO_2 composite. Tan et al[15] proposed that it was intrinsically correlated with the interdiffusion-induced interface movement of the aluminide/Ni toward the base alloy. The formation of Y-rich layer would retard the interdiffusion, and then influence the aluminization kinetics. In this case, sample Y1 exhibits the thickest $TiAl_3$ layer and highest thickness ratio of $TiAl_3/NiAl_3$. At the same time, the dispersion of Y-rich particles retards the grain growth of the aluminide coating, which leads to a finer-grain structure[10-13].

2.2 Oxidation

Fig.3 shows the isothermal oxidation curves of Y0, Y0.5 and Y1 alloys. It can be concluded that no spallation occurs in Y0, Y0.5 and Y1 alloys according to Fig.3a. In contrast, a significant mass loss occurs for Y5 when the oxidation time is 5 h, due to severe spallation, which can also be seen by naked eye. Thus, its oxidation kinetics is not plotted in Fig.3. Clearly, Y0 and Y0.5 alloys both obey a parabolic rate law to a good approximation for the whole duration of the test. However, for Y1 alloy, two regimes parabolic law

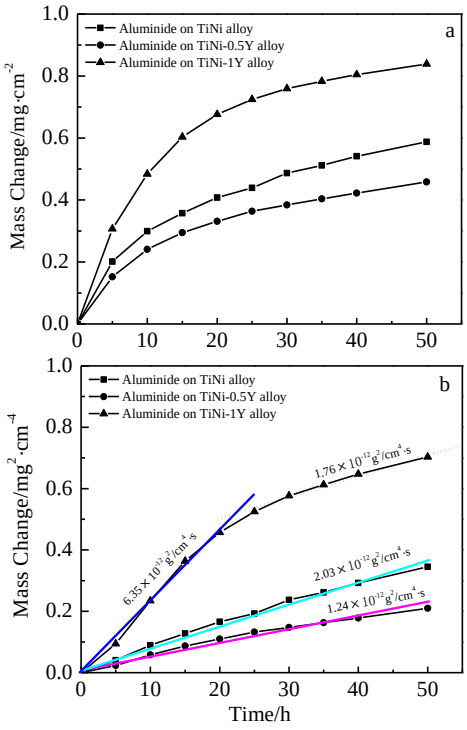

Fig.3 Isothermal oxidation curves of various samples in air at 700 ℃ for 50 h

occurs. The calculated parabolic oxidation rate constants are also given in Fig.3b. Comparing Y0 alloy and Y0.5 alloy with Y1 alloy, the formers exhibit lower oxidation kinetics, but the latter exhibits higher oxidation rate. This result suggests that the addition of minor amount of rare earth Y improves the oxidation resistance, but the addition of higher amount of Y element decreases the oxidation resistance.

Y0, Y0.5 and Y1 alloys with 50 h oxidation at 700 ℃ in air were characterized using XRD and the results are presented in Fig.4. The results indicate that all samples have grown a protective scale of alumina in α and θ Al_2O_3 forms besides minor rutile being detected in Y0 alloy. From Fig.4, it can be also found that the phases of three aluminide coatings after oxidation are almost Ni_2Al_3 with minor $TiAl_3$. However, Y0 and Y0.5 alloys exhibit higher peak intensity of $TiAl_3$ phase, especially the later. This suggests that the addition of 0.5 at%Y significantly delay the degradation of aluminide coatings, but the addition of 1at%Y accelerate the degradation.

To clarify the difference in the oxidation performances of various samples, surface and cross-sectional morphologies of the scales formed were investigated.

Fig.5 reveals the SEM top-views of the scales formed on different samples after 50 h exposure in air at 700 ℃, showing a similar whisker/blade and round-shape crystals except a small amount of Ti-rich fibriform on the surface of

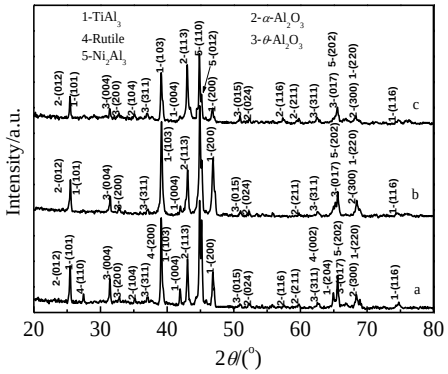

Fig.4 XRD patterns of various samples after isothermal oxidation at 700 ℃ for 50 h: (a) Y0, (b) Y0.5, and (c) Y1

Y0 alloy. Based on the XRD and previous results[10-13], the whisker/blade-like crystal is θ-Al_2O_3, the round crystal is α-Al_2O_3 but the Ti-rich fiber-shaped is rutile phase. Compared with Y0.5 alloy, the growth of θ-Al_2O_3 phase on Y0 and Y1 alloys is significantly inhibited, especially Y1 alloy. This can be seen clearly in Fig.5. Both the grain size and volumetric fraction of whisker/blade-like θ-Al_2O_3 are reduced. This implies that the faster θ-α phase transformation occurs on Y0 and Y1 alloys than that on Y0.5 alloy.

Fig.6 shows the corresponding cross-sections of the oxide scales. It can be found that thicker alumina scales are formed on Y0 and Y1 alloys, as seen in Fig.6a and Fig.6c. However, for Y0.5 alloy, thinner scales can be observed, as seen in Fig.6b. From the inset in Fig.6c, it can be found that some oxide nodules penetrate into the aluminide coating along the bright Y-rich particles, suggesting that the inner diffusion of oxygen along the bright Y rich particles occurs.

From the XRD results presented in Fig.1 and Fig.4, it can be seen that the degradation of $TiAl_3$+$NiAl_3$ to Ni_2Al_3 with minor $TiAl_3$ occurs, due to Al consumption by oxidation and also by interdiffusion. In order to understand the degradation, elemental profiles of samples after 50 h oxidation in air were conducted using EDS. The result is presented in Fig.7. Clearly, the interdiffusion causes the formation of a 6~8.5 μm-thick interdiffusion zone, as shown in the inserted photo in Fig.6a and Fig.6b. Furthermore, it can be divided into "Ⅳ" and "Ⅴ" regions with different thickness, as listed in Table 1. Region "Ⅳ" is formed due to the penetration of Ti from the Ti-Ni into the aluminide coatings, whereas region "Ⅴ" is formed as a result of diffusion of Al from the aluminide coating into the Ti-Ni substrate. Moreover, the outward diffusion of Al due to oxidation also causes the formation of a 12~22 μm-thick regions, as termed in Fig.6 as "Ⅵ". From Table 1, it can be found that the thickness of interdiffusion zone reduces with the increase of Y content, suggesting the addition of Y retards the interdiffusion. However, the thickness of "Ⅵ" region decreases first and then increases with the increase of Y content, suggesting the degradation due to oxidation more heavily occurs on Y0 and Y1 alloys than that on Y0.5 alloy, which is consistent with the oxidation kinetics curves in Fig.3.

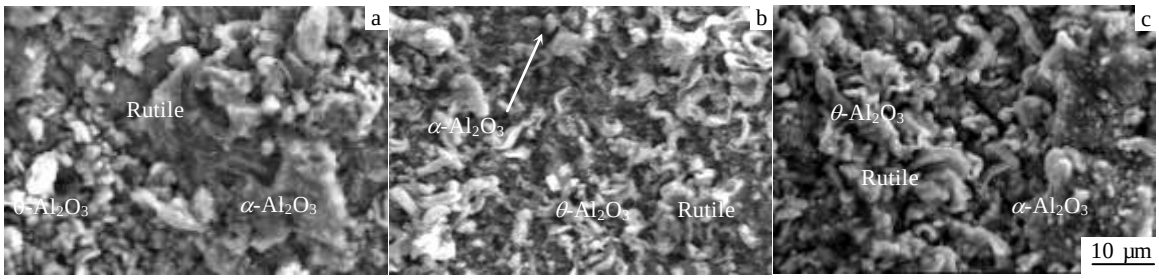

Fig.5 Surface morphologies of the oxides scales formed on different aluminide coatings: (a) Y0, (b) Y0.5, and (c) Y1

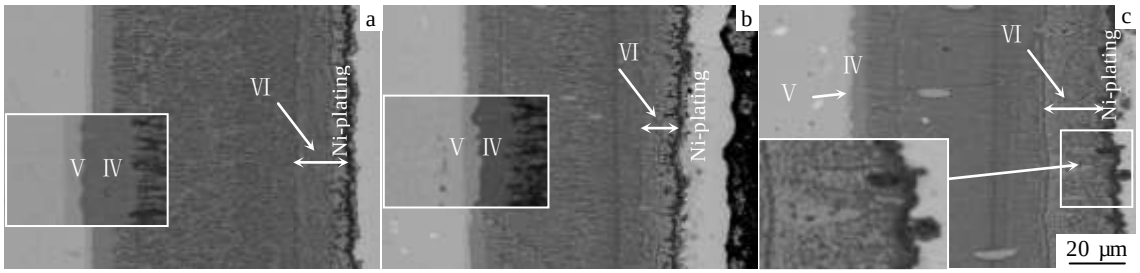

Fig.6 Cross-sectional morphologies of the oxides scales formed on different aluminide coatings after 50 h oxidation at 700 ℃ in air: (a) Y0, (b) Y0.5, and (c) Y1

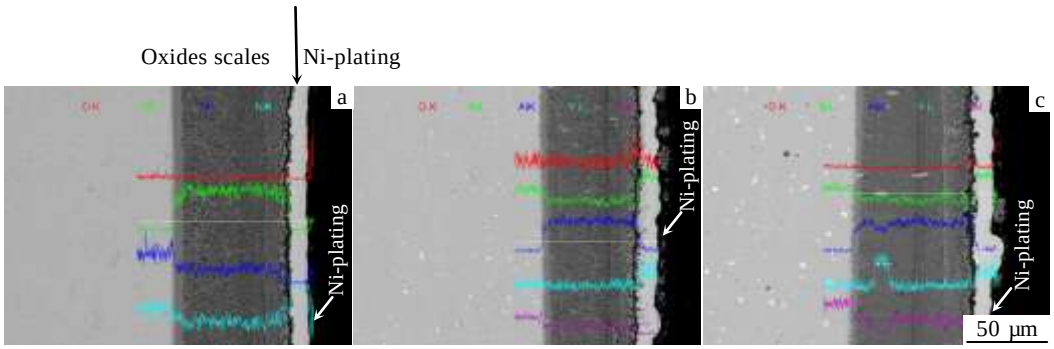

Fig.7 Cross-sectional SEM images and elemental depth profiles of different aluminide coatings after 50 h oxidation at 700 ℃ in air: (a) Y0, (b) Y0.5, and (c) Y1

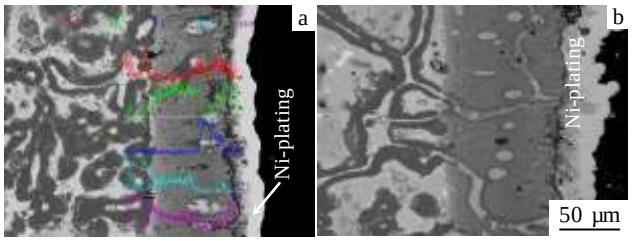

Fig.8 Cross-sectional SEM images and elemental depth profiles of aluminide coating formed on Y5 after 50 h oxidation at 700 ℃ in air: (a) a mixture of net-like TiO_2+γ-Ni and (b) oxidation deepening into Ti-Ni substrate

Fig.6c indicates that the oxidation along the NiY particles occurs due to inner diffusion of oxygen. With higher Y addition, the oxidation of NiY particles should deepen across the aluminide coating into the Ti-Ni substrate. To confirm this assumption, the cross section and element profile of Y5 alloy after oxidized at 700 ℃ for 50 h was analyzed, as shown in Fig.8b. Clearly, the oxidation along NiY particles may deepen across the aluminide coatings into Ti-Ni substrate. In this case, the oxidation of Ti-Ni substrate occurs. Because Ti is easily oxidized while Ni is more difficult to be oxidized[16], a mixture of netlike TiO_2 and γ-Ni with Ti solution formed in the Ti-Ni substrate, as shown in Fig.8a.

For the aluminide coatings, the oxidation rate is controlled by the air-coating interface reaction in the initial oxidation stage and the initial oxides are formed which have a great effect on the initial oxidation rate. It is well known that α-Al_2O_3 is a protective oxide with a slow growth rate, high stability and compact structure with few flaw, while θ-Al_2O_3 is a transient metastable oxide with a faster growth rate and more flaws. Previous results[17,18] also indicated that θ-alumina appeared in the outer part of the scale and α-alumina in the area close to the scale/metal interface. As further oxidized, θ-Al_2O_3 would gradually convert into slow-growing α-Al_2O_3. Therefore, the θ-Al_2O_3→α-Al_2O_3 transformation rate is one of the most important variables to influence the oxidation rate.

Many researches [11, 19-22] exhibited that different ions or its oxides had different effects on the θ-α transformation, and then influenced the oxidation rate. Burtin et al[19] and Fei et al.[22] found that TiO_2 had the same effect in accelerating θ-α transformation as a dopant does. From Fig.4 and Fig.5, it can be found that some local oxide TiO_2 is formed on the surface of Y0, which not only increases the oxidation rate, but also significantly accelerates the θ-α phase transformation. Due to large quantity of θ-alumina being formed and subsequently transformed into α-Al_2O_3 quickly in the initial oxidation stage[23], a much higher oxidation rate occurs. Moreover, the θ-α transformation causes an approximately 13.4% volume contraction. If the phase transformation is completed quickly, the tensile stress induced by the transient volume contraction may be large enough to give rise to micro-tears in the growing scale. Such micro-tears will lead to the fast growth of new oxides along the cracking surface, consequently increase the oxidation rate.

For Y0.5 alloy, due to the slow transformation from θ to α-alumina, the mass increase almost keeps a stable growth rate during oxidation. That is why Y0.5 alloy exhibits lower oxidation rate than Y0 alloy.

For Y1 alloy, the addition of Y has a great effect on the formation of stable α-Al_2O_3 and its oxidation rate, as addressed below. Firstly, the formation of Y_2O_3 oxides along Y-rich particles increases the initial oxidation rate. Secondly, because Y_2O_3 is an oxygen-deficient oxide, when the surface of the coating is covered with a high concentration of Y_2O_3, the oxygen transport through or around these particles might be accelerated[24]. Thirdly, due to large quantity of θ-alumina is formed and subsequently transformed into α-Al_2O_3 quickly in the initial oxidation stage[23], a much higher oxidation rate is occurs, as addressed above. That is why a high oxidation rate observed in the first 20 h. After 20 h, the formed Y_2O_3

particles on the surface, having the same crystallographic structure as α-Al_2O_3, provide an epitaxial template for this formation of α-Al_2O_3, thereby accelerating its formation. After the formation of a continuous protective α-Al_2O_3 scale, a lower oxidation rate can be observed, as shown in Fig.3.

For Y5 alloy, the oxidation of NiY particles deepens across the aluminide coating into the Ti-Ni substrate. In this case, the oxidation of Ti-Ni substrate occurs and a netlike TiO_2 is formed in the Ti-Ni substrate. The formation of netlike TiO_2 causes significant spallation of aluminide coatings.

The higher oxidation rate causes the faster degradation of the aluminide coatings (Fig.4). However, for Y5 alloy, due to higher content of Y, the formation of Y_2O_3 along NiY particles deepens across the aluminide coatings into Ti-Ni substrate(Fig.8). In this case, the oxidation of Ti-Ni substrate occurs and heavy spallation appears.

3 Conclusions

1) The aluminide coatings formed on Ti-Ni alloys with and without Y addition show a double layer structure: the outer $TiAl_3$ layer and inner $NiAl_3$ layer. And the aluminization progress is mainly controlled by inner diffusion of Al.

2) The addition of Y promotes the growth of outer $TiAl_3$ layer, but retards the growth of inner $NiAl_3$ layer when Y content is below 1at%.

3) The addition of 0.5at%Y significantly reduces the oxidation scale growth rate, but the addition of 1at%Y and 5at% Y significantly increase the oxidation rate.

References

1 Miyazai S, Otsuka K, Suzuki Y. *Scripta Metallurgica*[J], 1981, 15: 287

2 Kim K S, Jee K K, Kim Y B *et al*. *European Physical Journal-Special Topics*[J], 2008, 158: 67

3 Chu C L, Wu S K, Yen Y C. *Materials Science and Engineering A*[J], 1996, 216: 193

4 Xu C H, Ma X Q, Shi S Q *et al*. *Materials Science and Engineering A*[J], 2004, 371: 45

5 Okada M, Souwa M, Kasai T *et al*. *Applied Surface Science*[J], 2011, 257: 4257

6 Firstov G S, Vitchev R G, Kumar H *et al*. *Biomaterial*[J], 2002, 23: 4863

7 Liu A L, Sui J H, Lei Y C *et al*. *Journal of Materials Science*[J], 2007, 42: 5791

8 Pfeil L B. *UK Patent*, 459848[P]. 1937

9 Moon D P. *Materials Science Technology*[J], 1989, 5: 754

10 Xu C, Peng X, Wang F. *Corrosion Science*[J], 2010, 52: 740

11 Peng X, Guan Y, Dong Z *et al*. *Corrosion Science*[J], 2011, 53: 1954

12 Zhou Y B, Hu H T, Zhang H J. *Vacuum*[J], 2011, 86: 210

13 Zhang Haijun, Sun Jianfeng. *Rare Metal Materials and Engineering*[J], 2015, 44(11): 2628 (in Chinese)

14 Thaddeus B. *Binary Alloy Phase Diagrams, 2nd Edition*[M]. Ohio: ASM International, 1992: 2753

15 Tan X, Peng X, Wang F. *Surface and Coatings Technology*[J], 2013, 224: 62

16 Lee H G. *Chemical Thermodynamics for Metals and Materials* [M]. London: Imperial College Press, 1999: 275

17 Schumann E. *Oxidation of Metals*[J], 1995, 43: 157

18 Yang J C, Schumann E, Levin I *et al*. *Acta Materialia*[J], 1998, 46: 2195

19 Burtin P, Brunelle J P, Pijolat M *et al*. *Applied Catalysis*[J], 1987, 34: 225

20 Pint B A, Treska M, Hobbs L W. *Oxidation of Metals*[J], 1997, 47: 1

21 Kitajima Y, Hayashi s, Nishimoto T *et al*. *Oxidation of Metals*[J], 2010, 73: 375

22 Fei W, Kuiry S C, Seal S. *Oxidation of Metals*[J], 2004, 62: 29

23 Lee S Y, Lee J S, Kim K B *et al*. *Intermetallics*[J], 2003, 11: 743

24 Hou P Y, Shui Z R, Chuang G Y *et al*. *Journal of the Electrochemical Society*[J], 1992, 139: 1119

稀土元素 Y 对 TiNi 形状记忆合金基体渗铝涂层恒温氧化行为的影响

徐家文，刘爱莲，王永东，周月波

(黑龙江科技大学，黑龙江 哈尔滨 150022)

摘 要：采用粉末法，在不同Y含量的TiNi形状记忆合金基体上制备了650 ℃渗铝涂层，并对Y影响涂层的形成以及涂层在700 ℃恒温氧化性能进行了研究。结果表明：渗铝涂层由外层$TiAl_3$和内层$NiAl_3$构成，涂层的生长主要由Al的内扩散控制。当Y含量低于1at%时，稀土元素Y的添加促进$TiAl_3$外层的生长，抑制$NiAl_3$ 内层的生长。恒温氧化实验表明：添加0.5at%Y能明显降低渗铝涂层的氧化速度，但添加1 at%Y和5 at%Y却加速涂层的氧化。并对Y影响涂层的形成以及恒温氧化性能进行了分析。

关键词：TiNi 形状记忆合金；铝化物；恒温氧化；活性元素效应; 稀土 Y

作者简介：徐家文，男, 1975 年生，硕士，黑龙江科技大学材料科学与工程学院，黑龙江 哈尔滨 150022，电话：0451-88036159，E-mail: xujiawen@263.net